Article

Not peer-reviewed version

Effect of Main Bars of Beam on Shear Strength of Beam-Column Joint in Reinforced Concrete Frame Structure

Tianwen Dong * , Nobuaki Hanai , Toshiyuki Kanakubo

Posted Date: 9 March 2026

doi: 10.20944/preprints202603.0575.v1

Keywords: beam-column joint; main bars of beam; shear strength; shear force component; strut mechanism; diagonal compression strut

Article

Effect of Main Bars of Beam on Shear Strength of Beam-Column Joint in Reinforced Concrete Frame Structure

Tianwen Dong [1,*], Nobuaki Hanai [2] and Toshiyuki Kanakubo [3]

[1] Degree Program in Engineering Mechanics and Energy, University of Tsukuba, Tsukuba 305-8573, Japan
[2] Dept. of Architecture, Faculty of Architecture and Civil Engineering, Kyushu Sangyo Univ., Fukuoka 813-8503, Japan
[3] Dept. of Engineering Mechanics and Energy, University of Tsukuba, Tsukuba 305-8573, Japan
* Correspondence: s2536046@u.tsukuba.ac.jp

Abstract

In various countries, the shear strength design formulas for reinforced concrete beam–column joints are primarily constructed based on concrete strength, and the influence of main bars of beam is not explicitly reflected in these expressions. To address this limitation, this study examines the shear behavior of the joint, focusing particularly on the amount and arrangement of main bars of beam passing through the joint. Four beam-column joint specimens were tested under cyclic loading. The main variables of the specimens were the amount and arrangement of the main bars of beam. The detailed strain measurements were conducted to clarify the development of bond deterioration along the main bars and the associated internal force transfer mechanisms. The experimental observations revealed significant tension-shift phenomena and progressive bond deterioration in the compression-side main bars. Variations in the amount and arrangement of main bars of beam did not significantly affect the maximum applied load. However, the indirectly evaluated joint shear force was higher in specimens with two layers in beam main bars. Force equilibrium using force components obtained by measured strain produced even larger values at greater drift angles, indicating that joint shear assessment depends strongly on the evaluation basis. A mechanics-based diagonal strut model incorporating the internal compression field provided improved agreement with experimental results, confirming its applicability for practical design.

Keywords: beam-column joint; main bars of beam; shear strength; shear force component; strut mechanism; diagonal compression strut

1. Introduction

In reinforced concrete (RC) frames, the beam–column joint is one of the most critical structural components, as it connects the behavior of beams and columns and governs the overall lateral force-resisting mechanism of the frame. If the joint fails prior to the adjoining members, the load-carrying capacity and energy-absorption capability of the system deteriorate rapidly, potentially leading to collapse during an earthquake. Consequently, preventing shear failure of the joint has been recognized internationally as a fundamental requirement in seismic design [1–4].

Extensive earthquake damage observations and numerous experimental studies have repeatedly shown that the joint becomes a structural weak point. In the seismic design codes in various countries, the shear strength of the joint is predicted according to the joint geometry and boundary conditions, and shear force transmitted from the adjacent members must not exceed the shear strength of the joint. In Japan, the shear strength prediction in Architectural Institute of Japan (AIJ) design guideline [1] is based on the experimental results in which the shear strength is calculated by concrete strength, geometry and dimensions of the joint. The effects of internal reinforcement such as transverse reinforcement and main bars of beam passing through the joint are not explicitly incorporated.

The prediction formulas of shear strength of the joint in Japan, New Zealand, United States, and EU are summarized in Table 1.

In New Zealand, the seismic design of joints in NZS 3101 is based on the experimental and analytical studies by Paulay et al. [5], who proposed the diagonal compression strut and truss mechanism to express stress transfer mechanism within the joint. In this model, lateral force transmitted by bond action along the main bars of beam is considered to correspond to the shear force in column. The shear resistance in the joint is considered to be provided primarily by concrete and transverse reinforcement.

In United States, the design of joints in ACI 352R-02 originates from the experimental study by Meinheit and Jirsa [6] and was further developed by collecting experimental data from the USA, Japan, and New Zealand. This employs the mechanism models [7,8] that explicitly consider both main bars and transverse reinforcement. Unlike the New Zealand, it identifies concrete as the primary factor to shear resistance in the joint.

In EU, Eurocode 8 (EN 1998-1) [4] recommends a design approach based on a diagonal strut mechanism; however, in the absence of a more refined mechanical model, it follows an allowable-stress design concept similar to that of the AIJ Standard [9]. Furthermore, the influence of column axial force on joint shear strength is explicitly incorporated.

As summarized in Table 1, the joint shear strength design formulas adopted in various countries are primarily constructed based on the concrete strength. The influence of beam main bars is not explicitly reflected in these shear strength expressions. Likewise, previous studies based on mechanical models have mainly focused on the bond behavior of the main bars. Neither of these provisions in New Zealand nor the United States explicitly address how detailed main bars, such as the number of layers, quantity, or placement of beam main bars affect the formation of diagonal struts or the joint shear-resisting mechanism.

The review of past experimental results by Murakami et al.[10] reported that shear strength of the joint is governed primarily by concrete strength, while the influences of axial force in column, transverse reinforcement, and aspect ratio of the joint are comparatively ignorable. However, there is a tendency that shear strength of the joint increases as the ratio of tensile main bars in beams and columns also increases. Teraoka et al.[11] and Kusakari et al.[12] proposed the prediction formulas that include the effect of transverse reinforcement and main bar ratios., In the proposed mechanism, however, it is not clearly explained how the main bars of beam influences the shear strength of the joint. Morita et al.[13] also examined the influence of main bars of beam. However, the focus has been on the bond behavior of the beam main bars and the axial force in columns, and no detailed investigation has been conducted on the effect of the beam main bar arrangement on the shear strength of the joint.

Lin [14] conducted analytical and experimental studies varying the axial force in column, main bars layout in beam, and transverse reinforcement ratio. Though he reported that main bars layout influences the ductility of the joint, multiple factors such as the amount and arrangement of main bars, axial force and transverse reinforcement are treated as parameters, making it difficult to directly compare the results. In addition, not all specimens showed shear failure of the joint.

Kusuhara et al. and Shiohara [15–18] reported that some joint specimens cannot be conservatively evaluated using conventional shear-strength formulas and developed a nine-degree-of-freedom joint model based on bending theory to examine the internal stress state within the joint. The effect of the main bars and transverse reinforcement in the joint on the strength was shown, and it was pointed out that the amount of reinforcement in the joint design in Japan was insufficient. Furthermore, they explained the validity of the experimental results using the proposed model.

As described above, previous studies that have examined the influence of main bars of beam on the shear strength of the joint are limited, and there remain unclear aspects in the discussions regarding its effects.

 doi:10.20944/preprints202603.0575.v1

Based on the above background, loading test are conducted on beam-column joint specimens in which the amount and arrangement of main bars of beam passing through the joint are test variables. The objectives are to clarify how test variables influence the shear strength of the joint and to check the adaptability of shear-strength evaluation method focusing on the diagonal strut mechanism. Finally, by comparing the experiment results with the calculations by existing design codes, the applicability and limitations of the evaluation formulas are discussed.

Table 1. Design code of shear strength of joint in various countries.

<table>
<tr><th rowspan="2">Country</th><th rowspan="2">Shear strength prediction formula</th><th colspan="5">Influencing factor</th></tr>
<tr><th>Concrete strength</th><th>Geometry</th><th>Main bars</th><th>Reinforcement</th><th>Axial force</th></tr>
<tr><td>Japan (AIJ Design Guidelines)</td><td>$k\,f\,F_j\,b_j\,D_j$</td><td>Empirical coefficients based on experiment</td><td rowspan="2">Interior and exterior joints are classified.</td><td rowspan="4">Anchorage and bond performance of beam main bars passing through the joint are specified.</td><td>Minimum transverse reinforcement ratio is specified.</td><td rowspan="3">Not considered.</td></tr>
<tr><td>New Zealand (NZS3101)</td><td>$0.2\,f_c'\,b_j\,h_c$</td><td>Based on stress transfer mechanism</td><td>Structural provisions both transverse and longitudinal reinforcement are specified.</td></tr>
<tr><td>USA (ACI 352-R-02)</td><td>$\gamma\sqrt{f_c'}A_j$</td><td>Based on experiment</td><td>Classification is based on how many surfaces of the joint are restrained.</td><td>The cross-sectional area of the transverse reinforcement is specified.</td></tr>
<tr><td>EU (EC8)</td><td>$\eta f_{cd}\sqrt{1-\frac{v_d}{\eta}}b_j h_{jc}$</td><td>Based on the allowable-stress design concept</td><td>Interior and exterior joints are classified.</td><td>Adequate confinement of the joint is noted.</td><td>Normalized axial force in column is considered.</td></tr>
</table>

where,

k : coefficients depending on the geometry
f : correction coefficient depending on whether or not there is a orthogonal beam
F_j : ($=s_B^{0.7}$) standard value for joint shear strength
s_B, f_c', f_{cd} : concrete compressive strength
b_j : effective width of joint
D_j : effective depth of joint
h_c : depth of column
g : shear strength factor
A_j : effective area of joint
h : $=0.6(1-f_{ck}/250)$
f_{ck} : concrete compressive strength
V_d : normalized axial force in the column
h_{jc} : distance between extreme layers of column reinforcement

2. Experimental Program

2.1. Test Specimens and Materials

Four RC beam–column joint specimens were fabricated and tested. Table 2 shows the list of specimens. The shapes, dimensions, and reinforcement details of the specimens are shown in Figure 1. The assumed RC frame has a span of 2500 mm and a story height of 2250 mm, corresponding to about 1/3 scale model of an actual structure. To prevent failure of the beams and columns and to focus on the failure of the joint, high-strength reinforcing bars were used for the main bars, and sufficient stirrups and hoops were arranged. The main variables of the specimens are the amount and arrangement of the main bars of beam. Specimens 0D-T-A and 0D-T-P have three D16 bars as main bars, while Specimens 0D-T2-P and 0D-TA-P have five D16 bars. The detailed reinforcement arrangements of Specimens 0D-T2-P and 0D-TA-P are shown in Figure 2. To investigate the influence of the main bar arrangement on the shear strength of the joint, two of the main bars of 0D-TA-P were placed near the center of the beam cross-section that would not normally be adopted in practical design.

The mechanical properties of the reinforcing bars and concrete used in the specimens are summarized in Table 3. High-strength D16 and D13 bars were used as main bars for the beams and columns, respectively. D4 bars were used for the stirrups and hoops. The target compressive strength of the concrete mixture was 24 MPa, and the measured compressive strengths obtained from compression test on 100*f* x 200 mm cylinder specimens ranged from 23.8 to 25.7 MPa.

Table 2. list of specimens.

Specimen ID		0D -T-A	0D -T-P	0D-T2-P	0D-TA-P
Span length × Story height		2500×2250mm			
Beam	Width ×Depth	150×300mm			
	Main bars	3-D16		3+2-D16	3+2-D16
	Stirrups	◫D4@33, p_w=1.12%			
Column	Width ×Depth	180×300mm			
	Main bars	8-D13			
	Hoops	◫D4@33, p_w=0.94%			
	Joint	□D4@50, p_{jw}=0.31%			
Loading		Reversed cyclic	Oneway cyclic		

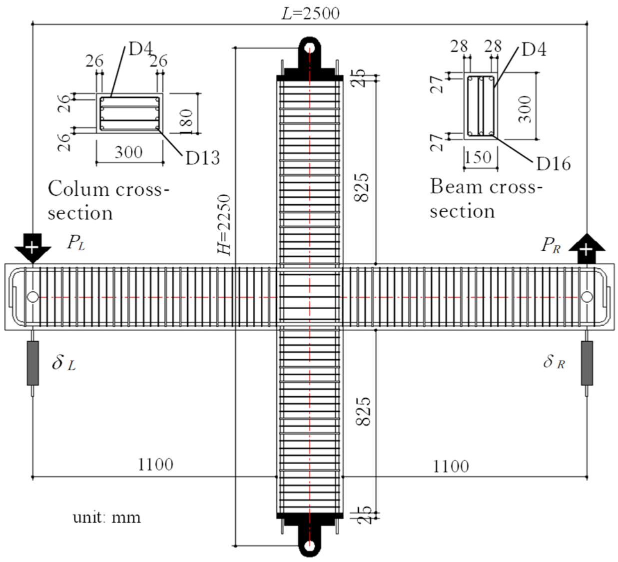

Figure 1. Dimensions and reinforcement details of specimens 0D-T-A and 0D-T-P.

 doi:10.20944/preprints202603.0575.v1

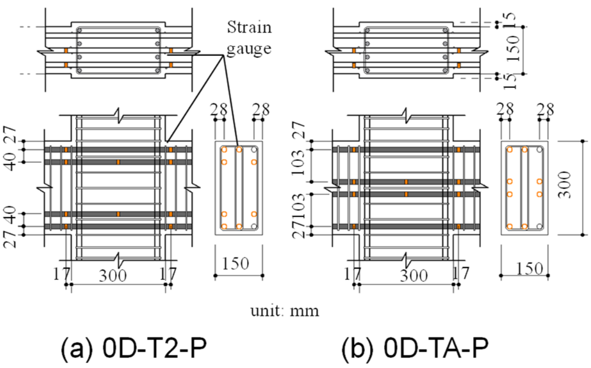

Figure 2. Joint details of specimens 0D-T2-P and 0D-TA-P.

Table 3. Mechanical Properties of reinforcing bars and concrete.

Reinforcing bar	ID	yield strength (MPa)	Young's modulus (GPa)
	D13	831(866)	203(210)
	D16	824(831)	214(211)
	D4	379(399)	195(191)
Concrete	Compressive strength (MPa)	Tensile strength (MPa)	Young's modulus (GPa)
	23.8(25.7)	2.39(2.38)	24.7(25.4)

( ): specimen 0D-T-A.

2.2. Loading and Measurement

The loading setup is shown in Figure 3. The column top and bottom were pin-supported, and a pair of actuators applied antisymmetric displacements for beams at points located 1100 mm from each column face. Specimen 0D-T-A was subjected to fully reversed cyclic loading, while the remaining specimens were subjected to oneway cyclic loading as that each cycle was unloaded to zero before proceeding to the next cycle.

The drift angle was calculated as the sum of the left and right actuator displacements divided by the span length (2500 mm). No axial load was applied to the column.

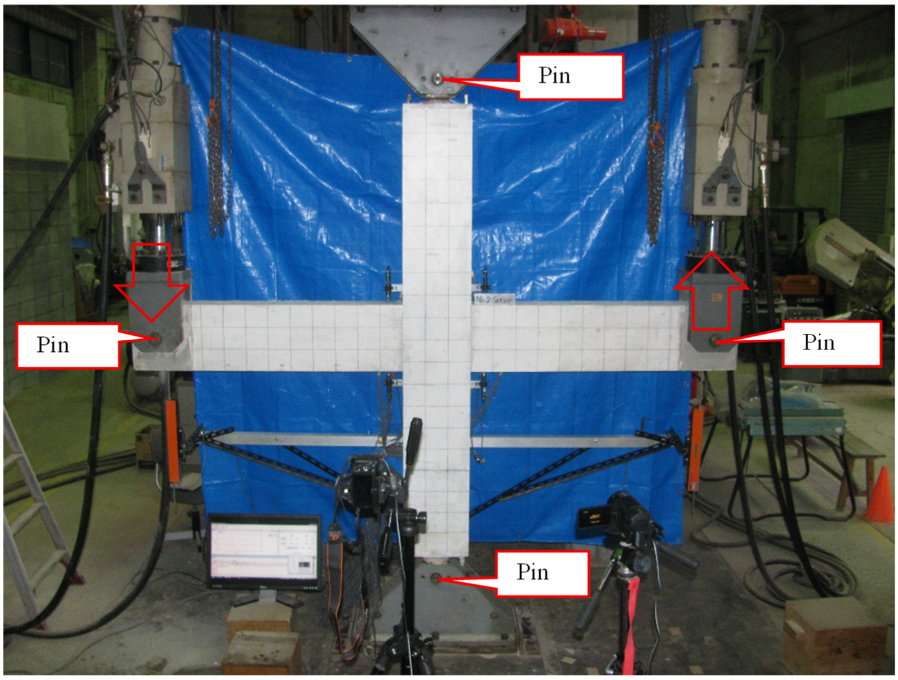

Figure 3. Loading setup.

3. Test Results

3.1. Applied Load–Drift Angle Response and Failure Mode

Figure 4 shows the applied load (P_{exp}) –drift angle (R) relationships, where P_{exp} is the average load of the two beam actuators. The maximum applied loads are also shown in the figure. Crack patterns and failure progress at R = 20x10^{-3} rad. and 40 or 67x10^{-3} rad. loading cycle are shown in Figure 5.

Specimen 0D-T-A exhibited bending cracks at the beam end at 2x10^{-3} rad. In positive loading, diagonal crack initiated within the joint at +10x10^{-3} rad., extending from the lower-left to upper-right corners in panel zone. In negative loading, a similar diagonal crack formed in the opposite direction. The maximum load was observed at ±20x10^{-3} rad. Severe diagonal cracks in the panel zone developed thereafter, followed by crushing near the beam compression zones. A sudden drop of the load occurred at −40x10^{-3} rad. when the cover concrete at the panel zone spalled off.

Specimen 0D-T-P showed a diagonal crack from the upper-right to lower-left of panel zone at 10x10^{-3} rad. and showed the maximum load at 20x10^{-3} rad. Cover-concrete spalling initiated at 30x10^{-3} rad., and severe crushing occurred beyond 40x10^{-3} rad. loading cycle.

Specimen 0D-T2-P exhibited diagonal cracks at 5x10^{-3} rad., whereas 0D-TA-P showed earlier cracking at 2x10^{-3} rad. Both specimens showed the maximum load at 20x10^{-3} rad. showing more extensive cracking and harsher crushing than those observed in 0D-T-P. After 40x10^{-3} rad. loading cycle, their failure patterns resembled that of 0D-T-P.

In all specimens, severe opening of the diagonal cracks and spalling of concrete in the panel zone cause the failure of the joint. No yielding of main bars both in beam and column was observed. It is recognized that all specimens failed by shear in the joint. The

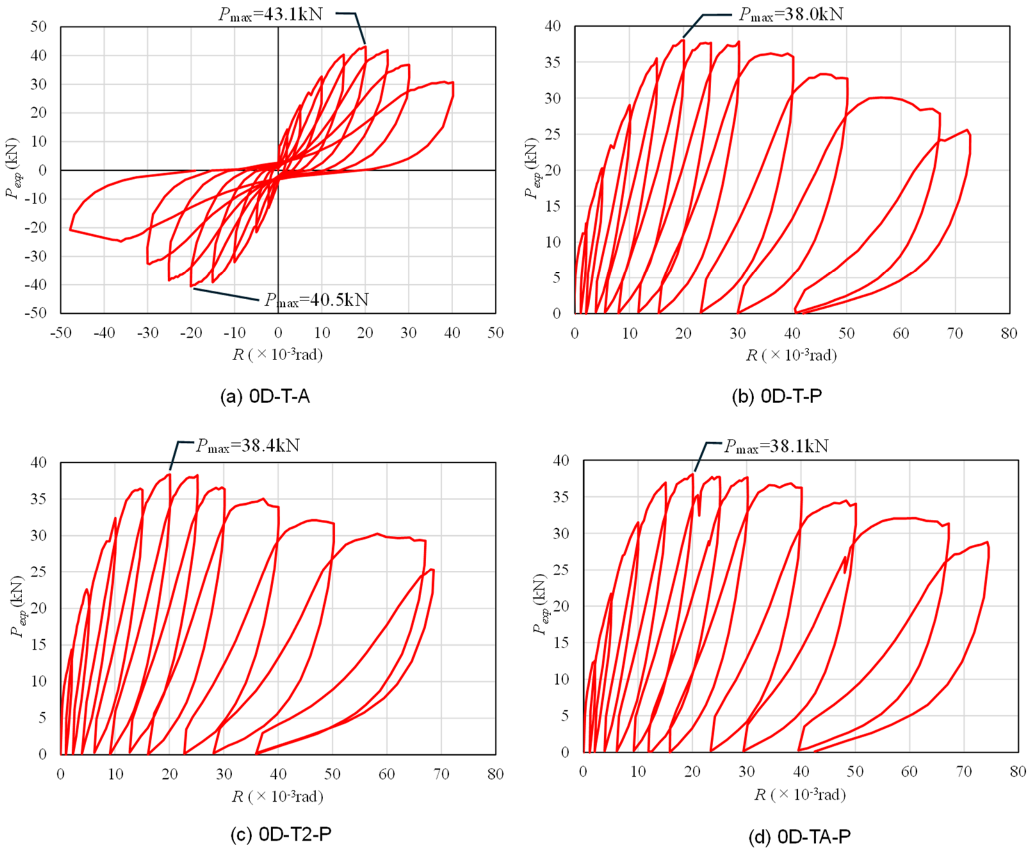

Figure 4. Applied load–drift angle relationship.

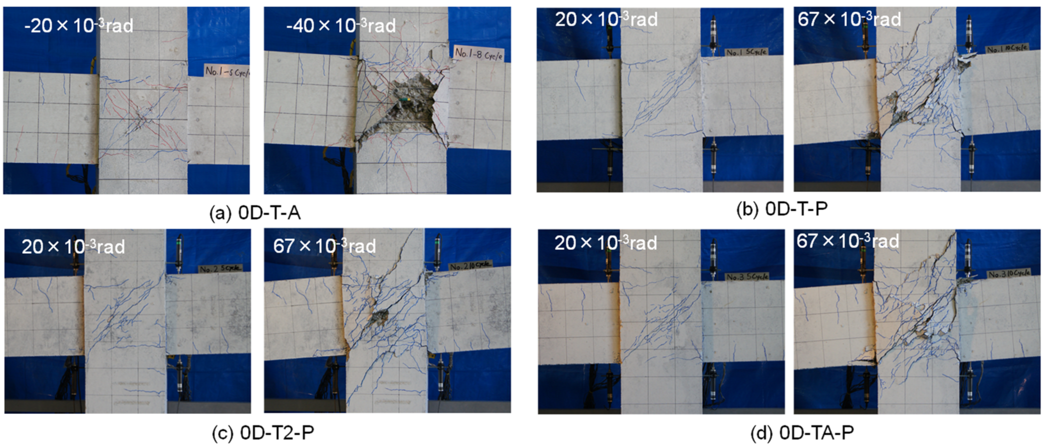

Figure 5. Crack patterns and failure progress.

specimens subjected to oneway loading showed similar maximum loads, while specimen 0D-T-A subjected to reversed loading resulted in more rapid degradation.

3.2. Strains of Main Bars

Figure 6 shows the strain distribution of main bars in specimen 0D-T-A. In positive loading (blue plots), steep strain gradients were observed between B6–B10 in main bar of beam, this indicates that large bond stresses are developing near the compression edge of the column. In negative loading (red plots), strain gradients in the same region were shallow, suggesting bond stress occurred in this region is small. It suggested that deterioration of the bond between the beam main bars occurred at the tensile edge of the column. Tensile strains were observed in compressive zone of beam, this is thought to be due to the bond deterioration occurring between B2 and B6 (B6 and B10), which resulted in the bond area shifting to the right (left) beam in positive (negative) loading. Shiohara et al. [19] also reported similar behavior and indicating "tension shift" due to bond deterioration in main bars.

Main bars in column exhibited tensile strains in compression zone as well. The strain gradients suggested almost uniform bond stress distribution in the panel zone.

Figure 7 shows strain distributions of the main bars of beam at the maximum load comparing the positions of main bars in specimens applied oneway cyclic loading. The strains of the first-layer bars plotted by void marks are assumed ones based on the strain distribution observed in the 0D-T-A specimen. Similar to the 0D-T-A specimen, tensile strains were observed in the main bars located within the compression zone at the beam ends of all specimens. Kusuhara et al. [20] pointed out that the tensile conversion of compression-side beam bars enlarges the concrete compression zone. Conversely, in cases such as the present experiments, where the beam main bars do not yield and the joint strength is governed by concrete compression within the joint, an increase in strut capacity enables the transmission of larger compressive forces, resulting in higher joint shear strength.

In the central bars of the 0D-TA-P specimens, similar strain levels can be observed at both beam ends and at the column center position, and their magnitudes were comparable to those of the first-layer bars on the beam bending tension side. In contrast to the second-layer bars in the 0D-T2-P specimen, where bond forces develop within the joint, the central-layer bars in the 0D-TA-P specimen do not mobilize bond stresses; instead, they are suggested to contribute to restraining the expansion of the joint core region.

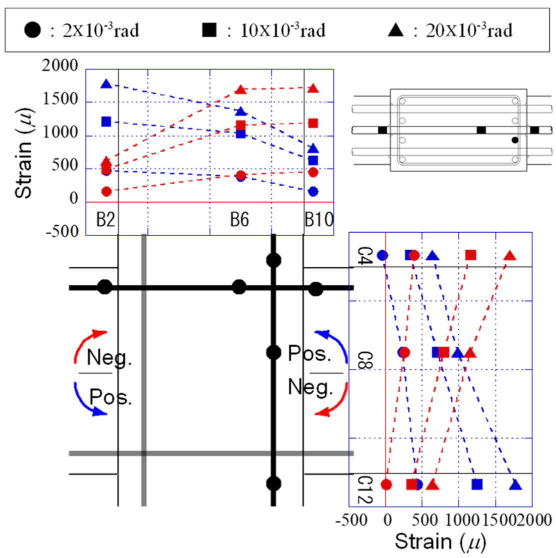

Figure 6. Strain distribution of main bars of specimen 0D-T-A.

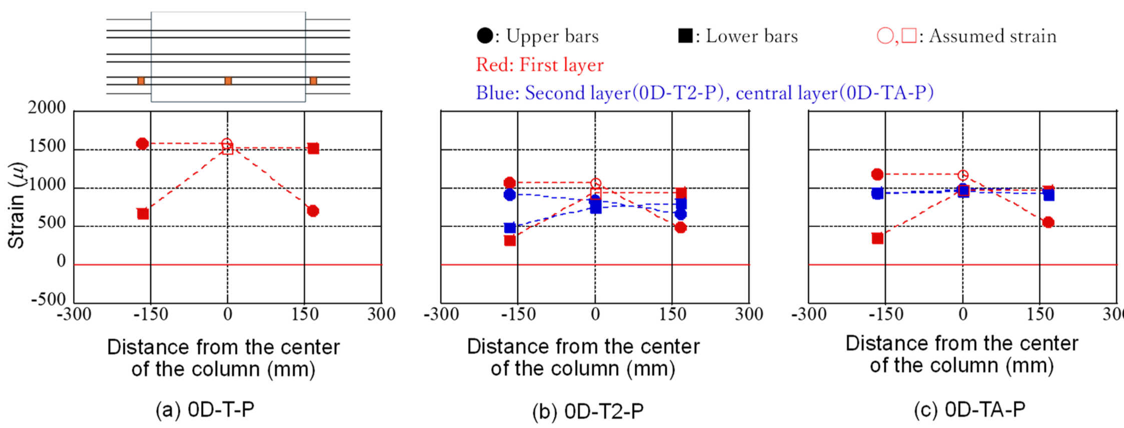

Preprints.org (www.preprints.org) | NOT PEER-REVIEWED | Posted: 9 March 2026 doi:10.20944/preprints202603.0575.v1

Figure 7. Strain distribution of main bars at the maximum load.

3.3. Force Components Acting in Panel Zone

Using the measured strain and material properties (Table 3), forces in each main bars layer (Equations (1) and (2)), concrete compression force (Equation (3)) and distance between the centers of stress resultants (Equation (4)) are calculated.

$$T_s = a_{st} E_s e_{st} \quad (1)$$

$$C_s = a_{sc} E_s e_{sc} \quad (2)$$

$$C_c = T_s - C_s \quad (3)$$

$$d_{cc} = (M_b + T_s d_{ts} + C_s d_{cs}) / C_c \quad (4)$$

where,

T_s: tensile force of main bars in tension side (Tension is taken as positive.)

C_s: compressive force of main bars in compression side (Compression is taken as positive.)

C_c: compressive force of concrete (Compression is taken as positive.)

d_{cc}: centroid of the concrete compressive stress distribution

a_{st}, a_{sc}: cross-sectional area of tension and compression main bars

E_s: Young's modulus of main bar

e_{st}, e_{sc}: measured strain of main bar (For the first-layer bars, the strain value was defined as the average of the strain gauge measurements taken from the main bars positioned at the left and middle of the beam cross section, as shown in Figure 2.)

M_b: beam bending moment of beam at column face

d_{ts}, d_{cs}: distance of tension/compression main bars to compression edge

Figure 8 shows the force components acting in panel zone at R=20x10^{-3}rad. of the joint. For the 0D-T2-P and 0D-TA-P specimens, the bending moments at the beam ends are similar, but the bond force generated in the first-layer bars is similar for both specimens. The tensile force in the central-layer bars of the 0D-TA-P specimen is greater than that in the second-layer bars of the 0D-T2-P specimen, and the concrete compressive force in the 0D-TA-P specimen is also greater.

Two methods are used to obtain the assumed shear force acting in the joint: (1) an indirect method based on the beam-end moments and effective depth commonly used in the design, and (2) a force equilibrium using force components obtained by measured strains. The calculations for these two methods are given in Equations (5) and (6), respectively.

$$V_{jexp1} = \frac{{}_{L}M + {}_{R}M}{j_b} - V_c \quad (5)$$

$$V_{jexp2} = T_s + C_s + C_c - V_c \quad (6)$$

where,

${}_{L}M$, ${}_{R}M$: bending moment of left/right beam at the beam end (=(L-D_c)/2・P_{exp})

L: span length

D_c: depth of column

P_{exp}: applied load (experimental value)

j_b: distance between the compressive and tensile forces of beam (=7/8d)

d: effective depth of beam (273 mm for 0D-T-P and 0D-TA-P, 257 mm for 0D-T2-P)

V_c: column shear force (=L/H・P_{exp})

H: story height

T_s: tensile force of main bars in tension side (Tension is taken as positive.)

C_s: compressive force of main bars in compression side (Compression is taken as positive.)

C_c: compressive force of concrete (Compression is taken as positive.)

Figure 9 compares two assumed shear forces acting in panel zone plotting the values at each loading cycle peak.

V_{jexp2} consists of the bond force component (T_s+C_s), which is the sum of the forces in the main bars on the tensile and compressive sides of the beam, the concrete compressive force component (C_c), and the column shear force component (V_c). These are also shown in the figure.

For all specimens, V_{jexp2} exhibited a larger value than V_{jexp1}. While the beam load reached its maximum value at a cycle of 20×10^{-3} rad, V_{jexp2} reached its maximum value at a later cycle. At the same story drift angle, the bond force component of the first-layer bars in the 0D-T-P specimen is nearly equal to the bond force components of the first and second-layer bars in the 0D-T2-P specimen. The bond force components of the first-layer bars in the 0D-T2-P and 0D-TA-P specimens are nearly equal, while the bond force component of the central-layer bars in the 0D-TA-P specimen is smaller. Furthermore, the concrete compressive force component of the 0D-TA-P specimen is greater than that of the other specimens.

Table 4 shows the maximum applied load and shear force in panel zone. The maximum value of V_{jexp2} is approximately 3% greater for the 0D-T2-P specimen and approximately 9% greater for the 0D-TA-P specimen compared to the 0D-T-P specimen. Furthermore, while there is almost no difference in the maximum beam load between the 0D-T-P and 0D-T2-P specimens, the maximum value of V_{jexp1} is approximately 8% higher for the 0D-T2-P specimen. Thus, it is necessary to note that differences arise in structural performance evaluation depending on whether beam load or joint shear force is used as the basis.

From the above, the maximum joint shear force calculated from the bending moment and effective depths at the beam ends is evaluated higher for specimens with two layers of main bars compared to those with a single layer. Therefore, for estimating the shear strength of the joint, it is considered more appropriate to calculate it based on the stress state at the beam end rather than using the joint shear force calculated from the bending moment and effective depth at the beam end.

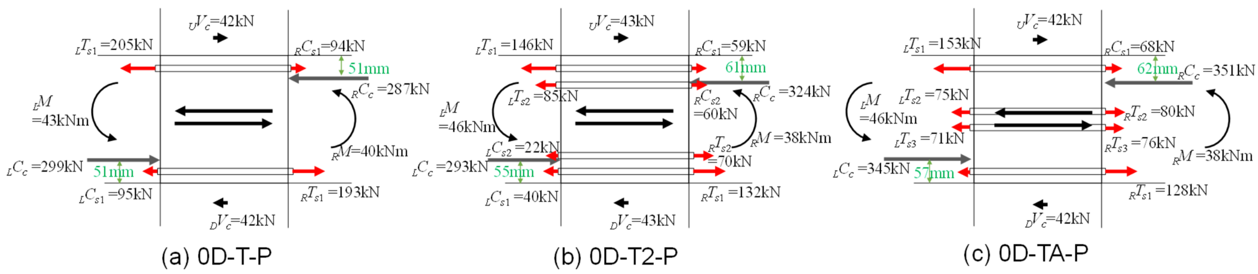

Figure 8. Force components acting in panel zone at R=20×10^{-3}rad.

Preprints.org (www.preprints.org) | NOT PEER-REVIEWED | Posted: 9 March 2026 doi:10.20944/preprints202603.0575.v1

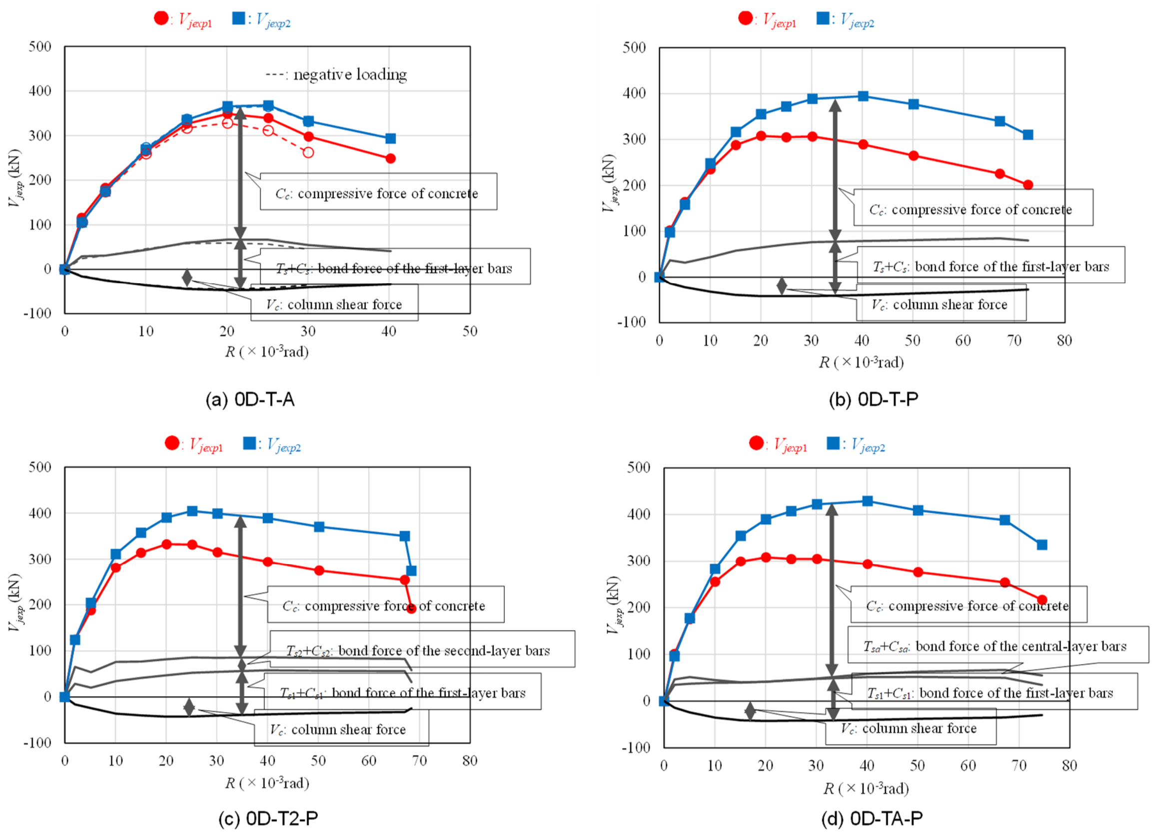

Figure 9. Assumed shear force progression acting in panel zone.

Table 4. Maximum applied load and maximum shear force in panel zone.

Test specimen	Maximum beam load (kN)		Maximum shear force (kN)			
	P_{expmax}	R(%)	V_{jexp1}	R(%)	V_{jexp2}	R(%)
0D-T-A	+43.1/-40.5	2.0	+349/-328	2.0	+366/-366	2.5
0D-T-P	38.0	2.0	308	2.0	394	4.0
0D-T2-P	38.4	2.0	333	2.0	405	2.5
0D-TA-P	38.1	2.0	308	2.0	429	4.0

4. Prediction of Shear Strength of the Joint

4.1. Influence of Beam and Column Main Bars on the Strut Mechanism

As shown in the previous chapter, the strain distributions of the beam and column main bars reveal the occurrence of “tension shift” in the compression-side, which clearly indicates degradation of bond stresses within the joint. Under such conditions, the contribution of the truss mechanism becomes significantly limited, and the diagonal concrete strut mechanism is expected to dominate the shear resistance.

Lee et al. [21], building upon the composite strut–truss model proposed by Paulay et al. [5], demonstrated that the shear strength of the joint is predominantly governed by the diagonal strut mechanism. Consistent with their findings, the present study focuses on the strut-resisting mechanism, considering the compression field within the joint.

Figure 10 illustrates the conceptual model of the diagonal compression strut formed within the joint. The shear resistance provided by this strut, denoted as V_{js}, is expressed by Equation (7).

$$Vjs = \sigma_{sc} D_s b_j \cos\theta \quad (7)$$

where,

σ_{sc}: principal compressive stress developed in the diagonal strut

D_s: effective depth of strut [$=(x_b + x_c \tan\theta)\cos\theta$]
b_j: effective width of joint [1]
θ : inclination angle of strut [θ =Arctan(D_b-x_b)/(D_c-x_c)]
x_c , x_b: neutral-axis depths of column and beam
D_c , D_b: depths of column and beam

The strut depth D_s is governed by the extent of the bending compression zones at the beam and column faces, which are evaluated using the neutral-axis depths x_b and x_c obtained from the sectional analysis described in Section 4.2.

For beams, an increase in the tension bars results in a deeper neutral-axis depth x_b , thereby enlarging the effective horizontal compression domain of the strut, expressed as (D_s /(D_c sinθ)). Consequently, the horizontal shear-resisting component of the strut increases.

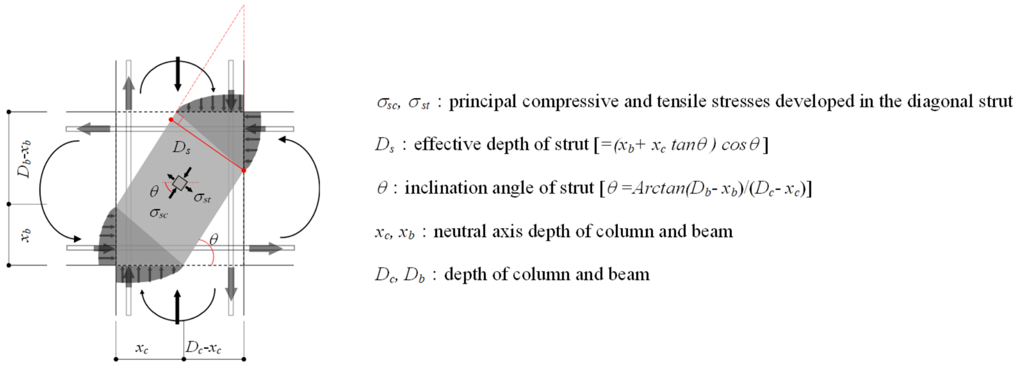

Figure 10. Conceptual diagonal concrete strut developed inside the joint core.

In contrast, the neutral-axis depth of the column x_c is influenced by both the column tension bars and the axial load level. While increases in either the tension bars or the axial load enlarge D_s , they also steepen the strut angle q, which reduces the horizontal component of the strut's compressive resistance. Nevertheless, the influence of these column-side factors is relatively minor compared with that of the beam tension bars. Therefore, the shear strength is governed primarily by the main bars of beam.

4.2. Evaluation of Shear Strength

Figure 4 To evaluate the formation and geometry of the diagonal strut within the joint, sectional analyses were conducted for the beam–column interface. The stress-strain relationships at the beam end were modeled as shown in Figure 11.

The neutral-axis depth x_n and curvature f were determined by simultaneously satisfying the following two equilibrium conditions:

1. Axial force equilibrium within the section
2. Moment equilibrium within the section

The obtained neutral-axis depth x_n is directly used in Section 4.1 for determining the effective strut depth D_s .

The sectional equilibrium conditions can be expressed as:

$$T_s+N= C_s+C_c \tag{8}$$

$$M = N(\frac{D}{2}\text{-}x_n)+T_s(d\text{-}x_n)+C_s(x_n\text{-}d_c)+\frac{bx_n^{\ 2}}{e_c^{\ 2}}\int_0^{e_c} f(e_c)\cdot e_c\cdot d(e_c) \tag{9}$$

where,

$$T_s=a_{st}\,E_s\,e_{st}$$
$$C_s=a_{sc}\,E_s\,e_{sc}$$
$$C_c=\frac{bx_n}{e_c}\int_0^{e_c} f(e_c)\cdot d(e_c)$$

T_s, C_s: tensile and compressive forces of main bars

Preprints.org (www.preprints.org) | NOT PEER-REVIEWED | Posted: 9 March 2026 doi:10.20944/preprints202603.0575.v1

C_c: compressive force of concrete
N: axial force
M: bending moment
D, b: depth and width of member
x_n: neutral-axis depth
d_c: distances to tension and compression bars
e_c: strain at the compression edge of concrete
a_{st}, a_{sc}: cross-sectional areas of tension and compression main bars
E_s: Young's modulus of main bar
e_{st}, e_{sc}: strain of main bar

The stress – strain relationships of the materials used in the analyses are shown in Figure 12. For concrete, the Sakino–Sun modified model [22] shown by Equation (10) was dopted to represent the nonlinear compressive stress–strain relationship, including the post-peak region. The main bars were modeled using a bilinear elastoplastic relationship based on the results of material tests, with the post-yield response idealized as perfectly plastic.

$$s_c = \frac{A\cdot\frac{e_c}{e_B}+(B\text{-}1)\left(\frac{e_c}{e_B}\right)^2}{1+(A\text{-}2)\cdot\frac{e_c}{e_B}+B\left(\frac{e_c}{e_B}\right)^2}\cdot s_B \tag{10}$$

where,

$A = E_c\, e_B / s_B$

$e_B = 0.94 \times s_B{}^{1/4} \times 10^{-3}$

B=2.25-0.017s_B [23]

e_B: strain at peak stress
E_c: Young's modulus
s_B: compressive strength

The analysis assumes that plane sections remain plane for both the beam and column members. For each specimen, an iterative convergence procedure is performed using Equations (8) and (9) to determine the curvature f and the neutral-axis depth x_n. The calculations are continued until the bending moment at the joint reaches its maximum value, corresponding to the joint strength of the joint V_{jexp2} listed in Table 4.

Figure 13 presents the neutral-axis depths at the beam ends for each specimen at the maximum shear force. For specimens 0D-T-A and 0D-T-P, which contained only a single layer of beam tension bars, the neutral-axis depth remained relatively shallow. In contrast, specimens 0D-T2-P and 0D-TA-P exhibited appreciably deeper neutral-axis positions, with nearly identical values for both specimens.

The compressive principal stress s_{sc} is assumed to reach the shear strength of the joint when it becomes equal to the effective compressive strength ns_B given by Equation (11) [24] within the strut. In addition, the transverse reinforcement in the joint core restrains crack propagation around the strut region, thereby enhancing the effective compressive strength that the strut can mobilize. This confinement effect is therefore incorporated into the evaluation of the joint shear resistance.

$$ns_B = 2.46 s_B{}^{0.70} + 1.74 p_{jw} s_{wy} + 5.02h - 0.82 \tag{11}$$

where,

s_B: compressive strength of concrete
p_{jw}: transverse reinforcement ratio within the joint (capped at 0.2% when exceeding this limit)
s_{wy}: yield strength of joint transverse reinforcement
h: axial load ratio applied to the column

Table 5 compares the shear strengths of the joint predicted by the strut mechanism comparing with the experimental strength V_{jexp}. Compared to the calculated value V_{js}, the experimental value V_{jexp2} is 2% to 16% larger, as shown in Table 5. This suggests that the shear strength of the joint can be appropriately evaluated based on the strut mechanism.

Table 5 also includes the calculated shear strength of the joint in Japan, New Zealand, United States, and EU codes. The shear strengths calculated using the design codes, it inherently provides a safety-side (conservative) evaluation.

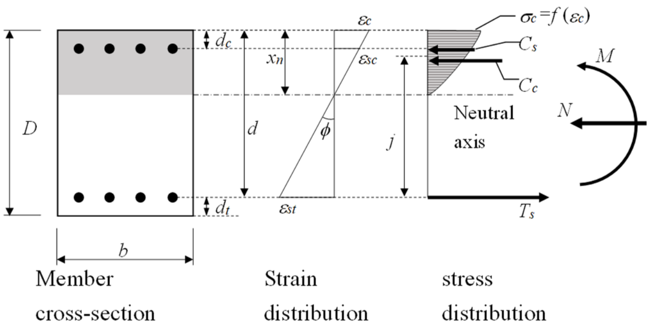

Figure 11. Assumed stress distribution in beam/column end section for sectional analysis.

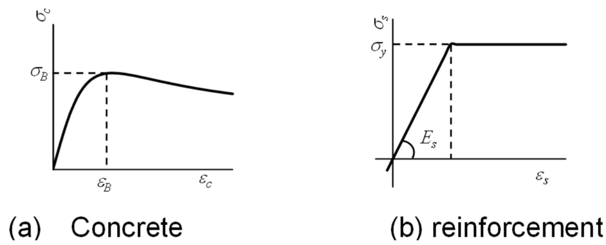

Figure 12. Stress–strain relationships used in analysis.

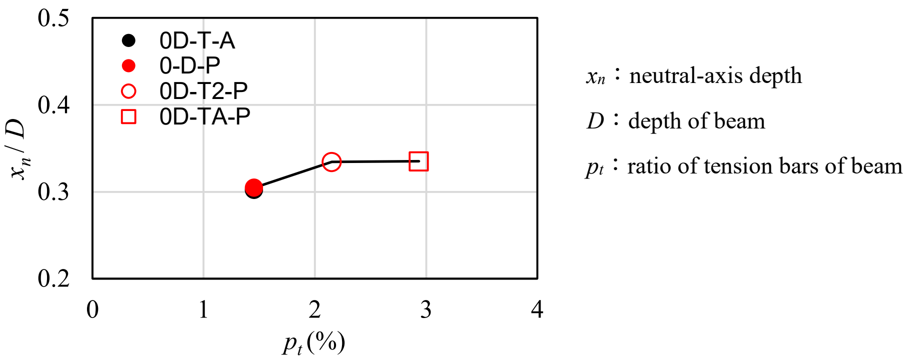

Figure 13. Neutral-axis depth at the maximum shear force obtained from sectional analysis for all specimens.

Table 5. Comparison of shear strength of the joint.

Specimen	Experimental value (kN)			Calculated strength (kN)			
	V_{jexp1}	V_{jexp2}	V_{js}	Japan (AIJ design Guidelines)	New Zealand (NZS 3101)	USA (ACI 352-R-02)	EU (EC8)
0D-T-A	349	366	358	327	278	250	412
0-D-P	308	394	342	310	257	241	385
0D-T2-P	333	405	368	310	257	241	385
0D-TA-P	309	429	369	310	257	241	385

 doi:10.20944/preprints202603.0575.v1

5. Conclusions

This study examined the shear behavior of beam-column joint focusing on the amount and arrangement of main bars of beam passing through the joint. Through the detailed strain measurements of the main bars and the associated internal forces transfer mechanism investigations, the evaluation of shear force acting in the panel zone and the diagonal compression strut mechanism were discussed. The major findings are summarized as follows:

(1) In all four specimens tested, severe opening of the diagonal cracks and spalling of concrete in the panel zone caused the failure of the joint without yielding of main bars. Variations in the amount and arrangement of main bars of beam did not significantly affect the maximum applied load.

(2) The results of strain measurement showed the bond deterioration in the beam main bars occurred at the tensile edge of the column. Tensile strains of main bars were observed in compressive zone of beam.

(3) The shear force acting in the panel zone was investigated by two methods, i.e., an indirect method based on the beam-end moments and effective depth commonly used in the design, and a force equilibrium using force components obtained by measured strains. The maximum shear force calculated by the former method showed greater ones for specimens with two layers of main bars compared to those with a single layer. For estimating the shear strength of the joint, it is considered more appropriate to calculate it based on the stress state by force components equilibrium.

(4) The shear strength of the joint was evaluated based on the diagonal compression strut model in which the dimensions of the strut were determined by the sectional analyses at the beam–column interface. The effective compressive strength of concrete proposed by the authors were adopted and the shear strength was calculated. The comparisons between the calculated values and the experimental ones suggests that the shear strength of the joint can be appropriately evaluated based on the strut mechanism.

Author Contributions: Conceptualization, N.H. and T.D.; methodology, N.H. and T.D.; formal analysis, T.D.; resources, N.H.; data curation, T.D.; writing—original draft preparation, T.D.; writing—review and editing, T.K. and N.H.; visualization, T.D.; supervision, T.K.; project administration, N.H.; funding acquisition, N.H. All authors have read and agreed to the published version of the manuscript.

Funding: This research received no external funding.

Data Availability Statement: Data are included in the paper.

Acknowledgments: In conducting this research, we received valuable assistance from Kyushu Sangyo University alumni Tomoyasu Hikichi and Yoshihiro Hiraoka, as well as invaluable advice from Professor Toshihiko Ninagawa of Kyushu University. We express sincere gratitude to them here.

Conflicts of Interest: The authors declare no conflicts of interest.

References

1. Architectural Institute of Japan (AIJ), Design Guidelines for Earthquake Resistant Reinforced Concrete Buildings Based on Inelastic Displacement Concept, AIJ, Tokyo, 1999.
2. NZS 3101: Concrete Structures Standard – Part 1: The Design of Concrete Structures, (Amendment 3, 2017)
3. ACI 352R-02: Recommendations for Design of Beam–Column Connections in Monolithic RC Structures, 2002.
4. EN 1998-1: Eurocode 8 – Design of Structures for Earthquake Resistance, Part 1: General Rules, Seismic Actions and Rules for Buildings, 2004
5. T. Paulay, R. Park, and M.J.N. Priestley.: Reinforced Concrete Beam-Column Joints Under Seismic Actions, ACI Journal, Vol.75, pp.585-593, 1978.11

 doi:10.20944/preprints202603.0575.v1

6. Donald F. Meinheit. and James O.Jisra.: The Shear Strength of Reinforced Concrete Beam-Column Joints, Final Report on a Research Project Sponsored by The National Science Foundation Research Grant GK-40289, Department of civil Engineering, University of Texas at Austin, Jan.1977
7. Zhang, L. and Jisra, J.O.: A study of Shear Behavior of Reinforced Concrete Beam-Column Joints, PMFSEL Report No.82-1, Department of civil Engineering, University of Texas at Austin, pp.118, Feb.1982
8. John Bonacci, Stavroula Pantazopoulou, Parametric Investigation of Joint Mechanics, ACI Structural Journal, V. 90, No. I, pp.61-71, 1993
9. Architectural Institute of Japan (AIJ), AIJ Standard for Structural Calculation of Reinforced Concrete Structures, AIJ, Tokyo, 2024.
10. Hideo Murakami, Shigeru Fujii, Yasuhiro Ishiwata and Shiro Morita: Shear Strength of Interior R/C Beam-Column Joint (Database study on beam–column joints Part 1), J. Struct. Censtr. Eng., AIJ, No.503, 85-92, Jan., 1998
11. Masaru Teraoka, Yoshikazu Kanoh and Katsumi Kobayashi: Study on the Shear Strength of RC Interior Beam-Column Joints－In the Case of Using Normal Concrete without Transverse Beams－, Journal of structural engineering, Vol. 37B, pp.365-392, 1991
12. Toshio Kusakari and Osamu Joh: A Study on Evaluation of Shear Strength of Reinforced Concrete Interior Beam-Column Joints Based on Experimental Data, Concrete Research and Technology, Vol. 9, No. 1, Jan. 1998
13. Shinji Morita, Kazuhiro Kitayama, Akio Koyama, Guki Hosono: Effect of Beam Main Bar Adhesion and Column Axial Force on the Shear Strength of RC Inner Column Beam Joints, Proceedings of the Japan Concrete Institute, Vol.21, No.3, pp.679-684, 1999
14. Cheng-Ming Lin: Seismic Behaviour and Design of Reinforced Concrete Interior Beam-Column-Joints Compressed, EQC project, No.97/294, 2001
15. Fumio Kushuhara, Hitoshi Shiohara, Wataru Tazaki and Sungyong Park: Seismic Performance of Reinforced Concrete Interior Beam-Column Joint under Low Ratio of Column Beam Moment Capacity, J. Struct. Constr. Eng., AIJ, Vol.75 No.656, 1873-1882, 2010
16. Hitoshi Shiohara: Reinforced Concrete Beam-Column Joint: Failure Mechanism Overlooked, J. Struct. Constr. Eng., AIJ, Vol.73 No.631, 1641-1648, 2008
17. Hitoshi Shiohara: Reinforced Concrete Beam-Column Joint: Interaction of Ultimate Strengths and Forces at Member Ends, J. Struct. Constr. Eng., AIJ, Vol.74 No.635, 121-128, 2009
18. Hitoshi Shiohara: Reinforced Concrete Beam-Column Joint: Seismic Design of Joints Connecting Weak Beams and Strong Columns, J. Struct. Constr. Eng., AIJ, Vol.74 No.640, 1145-1154, 2009
19. Hitoshi Shiohara, Safaa Zaid, Shunsuke Kotani: Interaction between Joint Shear Force and Anchorage Force in Beam-Column Joints, Proceedings of the Japan Concrete Institute, Vol.23, No.3, pp.355-360, 2001
20. Fumio Kusuhara, Hitoshi Shiohara: Causal Relationship Between Joint Shear Force and Joint Failure of RC Column Beam Joints Preceded by Joint Failure, Proceedings of the Japan Concrete Institute, Vol.19, No.2, pp.1005-1010, 1997
21. Lee Xianghao, Shunsuke Kotani: Shear Strength of Reinforced Concrete Inner Column Beam Joints, Proceedings of the Japan Concrete Institute, Vol.17, No.2, pp.303-308, 1995
22. Kenji Sakino and Yuping Sun: Stress –Strain Curve of Concrete Confined by Rectilinear Hoop, J. Struct. Constr. Eng., AIJ, No.461, 95-104, 1994
23. Fusheng Tian, Kenji Sakino and Yuping Sun: Effect of Strain Gradient on the Flexural Behavior of Confines R/C Columns, Journal of Structural Engineering, Vol.43B, pp. 191-198, 1973
24. Tianwen Dong: Discussion on Ultimate Shear Strength of Reinforced Concrete Beam-Column Joint with Different Levels on Beams, AIJ J.Technol.Des.Vol.31. No.88. 252-257, 2025